

Bound-state corrections in laser-induced nonsequential double ionization

C. Figueira de Morisson Faria^{1,2}, A. Sanpera¹ and M. Lewenstein¹

¹*Institut für theoretische Physik, Universität Hannover, Appelstr. 2, 30167 Hannover, Germany*

²*School of Engineering and Mathematical Sciences, City University,
Northampton Square, London EC1V 0HB, United Kingdom*

(Dated: July 6, 2019)

We investigate laser-induced nonsequential double ionization using a quantum-mechanical description of a physical process in which the second electron is freed by the inelastic collision of the first electron with its parent ion. In particular, we compute differential electron momentum distributions within the Strong-Field Approximation, employing a uniform saddle-point approximation, and introduce several technical modifications in order to improve the agreement between the outcome of this model and that of existing experiments. Such improvements include more realistic initial states for the second electron and an adequate treatment of the bound-state singularity which is present in the saddle-point framework. Although the changes in question do not lead to a better agreement with the experiments, they provide useful information about the influence of the initial states of both electrons. Indeed, we show that the momentum distributions are very sensitive with respect to spatially extended or localized wave functions, but are not considerably influenced by their shape. Furthermore, the modifications performed in order to overcome the bound-state singularity do not significantly alter the momentum distributions, apart from a minor suppression in the region of small momenta.

I. INTRODUCTION

Within the last few years, nonsequential double ionization in strong, linearly polarized laser fields has attracted a great deal of attention, both experimentally and theoretically [1]. This interest has been triggered by the outcome of experiments in which the momentum component parallel to the laser field polarization could be resolved, either for the doubly charged ion [2], or for both electrons [3]. Indeed, the observed features, namely two circular regions along the parallel momenta $p_{1\parallel} = p_{2\parallel}$ peaked at $p_{1\parallel} = p_{2\parallel} = \pm 2\sqrt{U_p}$, with U_p the ponderomotive energy, are a clear fingerprint of electron-electron correlation, and can be explained by a very simple, three-step rescattering mechanism. Thereby, an electron leaves an atom through tunneling ionization (the “first step”), propagates in the continuum, being accelerated by the field (the “second step”), and recollides inelastically with its parent ion (the “third step”). In this collision, it transfers part of its kinetic energy to a second electron, which is then released. Similar physical mechanisms are present in a wide variety of phenomena occurring in the context of atoms in strong laser fields, such as high-order harmonic generation [4, 5] and above-threshold ionization [6, 7], within classical [4, 6] and quantum-mechanical [5, 7] frameworks.

From the theoretical point of view, there exist models, both classical [8, 9, 10] and quantum-mechanical [11, 12, 13, 14, 15, 16, 17], based on such a mechanism, which qualitatively reproduce the above-mentioned features. They leave, however, several open questions. A very intriguing fact is that, for instance, a very good agreement with the experiments is obtained if the interaction through which the first electron is dislodged is of contact type, and if no Coulomb repulsion is taken into account in the final electron states. This agreement wors-

ens if this interaction is modeled in a more refined way, considering either a more realistic, Coulomb-type interaction, or final-state electron-electron repulsion. Specifically, in recent publications, such effects have been investigated in detail using both an S-Matrix computation and a classical ensemble model, and have been interpreted in terms of phase-space and dynamical effects [15, 16]. This analysis has been performed within the Strong-Field Approximation (SFA) [18], which mainly consists in neglecting the binding potential in the propagation of the electron in the continuum, the laser field when the electron is bound or at the rescattering, and the internal structure of the atom in question. We considered that the momentum components perpendicular to the laser field polarization are either arbitrary or limited to finite ranges.

In [16] we also found that the influence of the type of electron-electron rescattering, as well as of final-state Coulomb repulsion, is most pronounced if both transverse momenta are kept small. Furthermore, we have shown that a broadening in the momentum distributions in the direction perpendicular to $p_{1\parallel} = p_{2\parallel}$ is not necessarily a fingerprint of electron-electron repulsion, and may be caused by phase-space effects. Such investigations have been motivated by recent experiments, in which one of the electron momenta was resolved [19]. Therein, a similar broadening has been observed, and attributed to final-state Coulomb repulsion.

In the quantum-mechanical framework, the NSDI transition amplitude is written as a five-dimensional integral, with a time-dependent action and comparatively slowly varying prefactors. Such an integral is then solved using saddle-point methods. Apart from being less demanding than evaluating such an integral numerically [11, 12], or solving the time-dependent Schrödinger equation [20], these methods provide a clear space-time picture of the physical process in question, and are closely related to Feynman path integral methods. In particular, the re-

sults are interpreted in terms of the so-called “quantum orbits”. Such orbits can be related to the orbits of classical electrons in the continuum, and have been extensively used within the context of above-threshold ionization and high-order harmonic generation [21] as well as, more recently, nonsequential double ionization [14, 15, 16, 17].

The fact that, in [15, 16], the crudest approximation yields the best agreement with the experiments, seems to indicate that the presence of the residual ion, which is not taken into account, screens both the long-range interaction which frees the second electron and the final-state repulsion. This suggests that the presence of the ionic binding potential in the physical steps describing nonsequential double ionization, i.e., tunneling, propagation and electron-impact ionization, should somehow be incorporated. Indeed, in recent studies, it was found that Coulomb focusing considerably influences the NSDI yield [22].

Furthermore, it may as well be that an additional approximation performed in [15, 16] for the contact interaction, namely to assume that it takes place at the origin of the coordinate system, affects the shape of the momentum distributions, and contributes to the good agreement between theory and experiments in this case. Physically, this means that the spatial extension of the wave function of the second electron is neglected. Such an approximation has not been performed in the computations for the Coulomb interaction discussed in [15, 16], and, up to the present date, there exist no systematic studies of its influence in the context of NSDI.

In this paper, we take such effects into account in the simplest possible ways. First, we assume that both electrons are initially in hydrogenic $2p$ and in $3p$ states, instead of in s states, as previously done [14, 15, 16, 17]. One should note that, in contrast to Helium, for which s states are more appropriate, p states yield a more realistic description of the outer-shell electrons in neon and argon, respectively. Since the two latter species are used in most experiments, the choice of p states is justified. This is included in the transition amplitude as a form factor, and does not modify the saddle-point equations. In both p and s - state cases, we consider that the bound-state wave function of the second electron is either localized at the origin or extends over a finite spatial range, for the contact and Coulomb interactions.

A further improvement consists in overcoming the bound-state singularity, which is present in the saddle-point framework, and which has not been addressed in [15, 16]. For this purpose, we use a slightly modified action, with respect to that considered in [15, 16], so that the tunneling process and the propagation of both electrons in the continuum is altered. In particular, we perform a systematic analysis of how such corrections influence several features in the momentum distributions, such as their shapes, the cutoff energies or the contributions from different types of orbits to the yield.

The manuscript is organized as following. In Sec. II, we provide the necessary theoretical background for un-

derstanding the subsequent discussions. In Secs. III and IV, we present our results, and, finally, in Sec. V we state our conclusions.

II. BACKGROUND

A. Transition amplitude

The transition amplitude of the laser-assisted inelastic rescattering process responsible for NSDI, in the strong-field approximation, is given by

$$M = - \int_{-\infty}^{\infty} dt \int_{-\infty}^t dt' \langle \psi_{p_1, p_2}^{(V)}(t) | V_{12} U_1^{(V)}(t, t') \otimes V U_2^{(0)}(t, t') | \psi_0(t') \rangle \quad (1)$$

where V , $U_n^{(V)}(t, t')$, $U_n^{(0)}(t, t')$ and V_{12} denote the atomic binding potential, the Volkov and the field-free time evolution operators acting on the n -th ($n = 1, 2$) electron, and the interaction through which the second electron is freed by the first, respectively. Eq. (1) describes the following physical process. Initially, both electrons are bound, and the atom is in the product state $|\psi_0(t')\rangle = |\psi_0^{(1)}(t')\rangle \otimes |\psi_0^{(2)}(t')\rangle$, with $|\psi_0^{(n)}(t')\rangle = e^{i|E_{0n}|t'} |\psi_0^{(n)}\rangle$, ($n = 1, 2$). Thereby, $|E_{01}|$ and $|E_{02}|$ are the first and second ionization potentials, respectively [14, 15, 16]. Then, at the time t' , the first electron is released through tunneling ionization, whereas the second electron remains bound. Subsequently, the first electron propagates in the continuum from t' to t , gaining energy from the field. At this latter time, it collides inelastically with its parent ion, dislodging the second electron. The final electron state is taken either as the product state of one-electron Volkov states, or as a two-electron Volkov state, with asymptotic momenta p_1 and p_2 . The former and the latter case corresponds to the absence or presence of electron-electron repulsion in the final states, respectively. In this paper, we will concentrate on uncorrelated final states. For discussions of the influence of final-state Coulomb repulsion we refer to [11, 15, 16]. In Eq. (1), the Volkov states are taken in the length gauge. We use atomic units throughout.

If the Volkov time evolution operator is expanded in terms of Volkov states, Eq. (1) can be written as

$$M = - \int_{-\infty}^{\infty} dt \int_{-\infty}^t dt' \int d^3k V_{\mathbf{p}_n, \mathbf{k}} V_{\mathbf{k}, 0} \exp[iS(t, t', \mathbf{p}_n, \mathbf{k})], \quad (2)$$

with the action

$$S(t, t', \mathbf{p}_n, \mathbf{k}) = -\frac{1}{2} \sum_{n=1}^2 \int_t^{\infty} [\mathbf{p}_n + \mathbf{A}(\tau)]^2 d\tau - \frac{1}{2} \int_{t'}^t [\mathbf{k} + \mathbf{A}(\tau)]^2 d\tau + |E_{01}|t' + |E_{02}|t, \quad (3)$$

where $\mathbf{A}(t)$, \mathbf{p}_n , \mathbf{k} and $|E_{0n}|$ ($n = 1, 2$) denote the vector potential, the final momenta, the intermediate momenta and the ionization potentials, respectively. All the influence of the binding potential V and of the electron-electron interaction V_{12} is included in the form factors

$$V_{\mathbf{p}_n, \mathbf{k}} = \langle \mathbf{p}_2 + \mathbf{A}(t), \mathbf{p}_1 + \mathbf{A}(t) | V_{12} | \mathbf{k} + \mathbf{A}(t), \psi_0^{(2)} \rangle \quad (4)$$

and

$$V_{\mathbf{k}, 0} = \langle \mathbf{k} + \mathbf{A}(t') | V | \psi_0^{(1)} \rangle, \quad (5)$$

which are explicitly given by

$$V_{\mathbf{k}, 0} = \frac{1}{(2\pi)^{3/2}} \int d^3 r_1 \exp[i(\mathbf{k} + \mathbf{A}(t')) \cdot \mathbf{r}_1] V(\mathbf{r}_1) \psi_0^{(1)}(\mathbf{r}_1) \quad (6)$$

and

$$V_{\mathbf{p}_n, \mathbf{k}} = \frac{1}{(2\pi)^{9/2}} \int \int d^3 r_1 d^3 r_2 \exp[i(\mathbf{p}_1 - \mathbf{k}) \cdot \mathbf{r}_1] \times \exp[i(\mathbf{p}_2 + \mathbf{A}(t)) \cdot \mathbf{r}_2] V_{12}(\mathbf{r}_2, \mathbf{r}_1) \psi_0^{(2)}(\mathbf{r}_2), \quad (7)$$

respectively. The binding potential $V(\mathbf{r}_1)$ will be taken to be of Coulomb type, and the interaction $V_{12}(\mathbf{r}_2, \mathbf{r}_1)$ through which the second electron is released will be chosen to be of contact or Coulomb type. The initial state $\psi_0^{(1)}(\mathbf{r}_1)$ of the first electron at the moment of its ionization will be taken as a hydrogenic s or p state, and the wave function $\psi_0^{(2)}(\mathbf{r}_2)$ of the second electron at the moment of its release is either chosen as a hydrogenic state, or a Dirac delta state localized at $\mathbf{r}_2 = 0$.

B. Saddle-point analysis

For low enough frequencies and high enough laser intensities, Eq. (2) can be solved to a good approximation by the steepest descent method. Thus, we must determine \mathbf{k} , t' and t such that $S(t, t', \mathbf{p}_n, \mathbf{k})$ ($n = 1, 2$) is stationary, i.e., that its partial derivatives with respect to these variables vanish. This condition yields the equations

$$[\mathbf{k} + \mathbf{A}(t')]^2 = -2|E_{01}| \quad (8)$$

$$\sum_{n=1}^2 [\mathbf{p}_n + \mathbf{A}(t)]^2 = [\mathbf{k} + \mathbf{A}(t)]^2 - 2|E_{02}| \quad (9)$$

$$\int_{t'}^t d\tau [\mathbf{k} + \mathbf{A}(\tau)] = 0. \quad (10)$$

Eq. (8) gives the energy conservation during tunneling ionization, and, for a non-vanishing ionization potential, has no real solution. Consequently, t , t' and \mathbf{k} are complex quantities. In the limit $|E_{01}| \rightarrow 0$, Eq. (8) describes

a classical electron leaving the origin of the coordinate system with vanishing drift velocity. Eq. (9) expresses energy conservation at t , in an inelastic rescattering process in which the first electron gives part of its kinetic energy to the second electron, so that it can overcome the second ionization potential and reach the continuum. Finally, Eq. (10) yields the intermediate electron momentum constrained by the condition that the first electron returns to the site of its release. The saddles determined by Eqs. (8)-(10) always occur in pairs that nearly coalesce at the boundaries of the energy region for which the rescattering process is classically allowed. Such a boundary causes the yield to decay exponentially, leading to sharp cutoffs in the momentum distributions. If written in terms of the momentum components parallel and perpendicular to the laser field polarization, Eq. (9) reads

$$\sum_{n=1}^2 [p_{n\parallel} + A(t)]^2 = [\mathbf{k} + \mathbf{A}(t)]^2 - 2|E_{02}| - \sum_{n=1}^2 \mathbf{p}_{n\perp}^2 \quad (11)$$

and describes a hypersphere in the six-dimensional $(p_{n\parallel}, \mathbf{p}_{n\perp})$ space. For constant transverse momenta, Eq. (11) corresponds to a circle in the $(p_{1\parallel}, p_{2\parallel})$ plane centered at $-A(t)$ and whose radius is given by the difference between the kinetic energy $E_{\text{kin}}(t) = 1/2 [\mathbf{k} + \mathbf{A}(t)]^2$ of the first electron upon return and the effective ionization potential $|E_{02}| = |E_{02}| + \sum_{n=1}^2 \mathbf{p}_{n\perp}^2/2$. Hence, there is not only a maximal, but also a minimal energy for which electron-impact ionization is allowed to occur. Additionally, if $|E_{02}| < \sum_{n=1}^2 \mathbf{p}_{n\perp}^2/2$, this process will be classically forbidden throughout. In this paper, we will refer to the momentum regions within and beyond the cutoffs as the classically allowed and forbidden regions, respectively.

In the standard saddle point method, the transition amplitude is approximated by

$$M^{(\text{SPA})} = \sum_s A_s \exp(iS_s), \quad (12a)$$

$$S_s = S_{\mathbf{p}}(t_s, t'_s, \mathbf{k}_s), \quad (12b)$$

$$A_s = (2\pi i)^{5/2} \frac{V_{\mathbf{p}_n, \mathbf{k}_s} V_{\mathbf{k}_s 0}}{\sqrt{\det S''_{\mathbf{p}}(t, t', \mathbf{k})|_s}}, \quad (12c)$$

where the index s runs over the relevant saddle points and $S''_{\mathbf{p}}$ denotes the five-dimensional matrix of the second derivatives of the action with respect to t, t' and \mathbf{k} . In practice, this latter variable can be eliminated and the problem can be reduced to two dimensions, using Eq. (10) and the fact that the action (3) is quadratic in \mathbf{k} . Thus,

$$S_s = S_{\mathbf{p}}(t_s, t'_s, \mathbf{k}_s(t_s, t'_s)), \quad (13a)$$

$$A_s = (2\pi i)^{5/2} \frac{V_{\mathbf{p}_n, \mathbf{k}_s} V_{\mathbf{k}_s 0}}{\sqrt{(t_s - t'_s)^{3/2} \det S''_{\mathbf{p}}(t, t')|_s}}. \quad (13b)$$

The above-discussed saddle-point approximation is only valid for well-isolated saddles. This does not hold

near the boundaries of the classically allowed region, i.e., near the cutoffs, where the pairs of saddles nearly coalesce. Furthermore, beyond the classical cutoffs, one of the saddles yields exponentially increasing and therefore unphysical results, and must be discarded. This causes cusps in the cutoff region, which are particularly problematic for non-sequential double ionization (see, e.g., [14] for a discussion of this problem).

In this paper, we will use a more general, uniform approximation [26], which has been successfully applied in [24] to above-threshold ionization, in [25] to high-order harmonic generation, and in [14, 15, 16, 17] to NSDI, and whose only validity requirement is that the saddles occur in pairs. Within this approximation, for each pair of trajectories, the transition amplitude in the energy region for which electron-impact ionization is classically allowed is given by

$$\begin{aligned} M_{i+j} &= \sqrt{2\pi\Delta S/3} \exp(i\bar{S} + i\pi/4) \\ &\times \{ \bar{A}[J_{1/3}(\Delta S) + J_{-1/3}(\Delta S)] \\ &\quad + \Delta A[J_{2/3}(\Delta S) - J_{-2/3}(\Delta S)] \}, \\ \Delta S &= (S_i - S_j)/2, \quad \bar{S} = (S_i + S_j)/2, \\ \Delta A &= (A_i - iA_j)/2, \quad \bar{A} = (iA_i - A_j)/2. \end{aligned} \quad (14)$$

In the classically forbidden region, i.e., beyond the cutoffs, one of the saddles must be left out of the contour. For that purpose, one must take an appropriate functional branch of the Bessel functions, which will be chosen by imposing a smooth functional behavior at a Stokes transition. In the specific context of this paper, this transition marks a change in the asymptotic expansion of a function [23], and occurs at

$$\text{Re } S_{\mathbf{p}}(t_i, t'_i, \mathbf{k}_i) = \text{Re } S_{\mathbf{p}}(t_j, t'_j, \mathbf{k}_j). \quad (15)$$

For nonsequential double ionization, such transitions roughly coincide with the maximum and minimum classically allowed momenta, respectively. In the classically forbidden region the transition amplitude reads

$$\begin{aligned} M_{i+j} &= \sqrt{2i\Delta S/\pi} \exp(i\bar{S}) \\ &\times [\bar{A}K_{1/3}(-i\Delta S) + i\Delta AK_{2/3}(-i\Delta S)]. \end{aligned} \quad (16)$$

Equations (14) and (16) should be matched at the Stokes transitions. In the limit of well-isolated saddles, i.e., for $\Delta S \gg 1$, the standard saddle-point approximation is recovered from Eqs. (14) and (16). More details about this approximation are given in [24, 26, 27].

C. Momentum distributions

The momentum distributions of electrons for various types of interaction V_{12} and ranges of transverse momenta are then given by

$$M = \int d^2 p_{1\perp} \int d^2 p_{2\perp} |M_L + M_R|^2 \quad (17)$$

where M_L and M_R give the left and the right peak in the momentum distributions, respectively, computed using the uniform approximation. We consider a monochromatic, linearly polarized field, so that the vector potential reads

$$\mathbf{A}(t) = -A_0 \cos(\omega t) \mathbf{e}_x. \quad (18)$$

In this case, $M_R = M(t, t', p)$ and $M_L = M(t - T/2, t' - T/2, p)$, where $T = 2\pi/\omega$ denotes a period of the driving field. We use the symmetry property $|M(t, t', p)| = |M(t - T/2, t' - T/2, -p)|$ to compute the left peak. One should note that, for other types of driving fields, such as few-cycle pulses, this condition does not hold and each peak must be computed independently [10, 17].

III. INITIAL P STATES

Within the formalism discussed in the previous section, the first and second electron, so far, have been assumed to be initially in 1s- or zero-range-potential bound states, whose energies $|E_{01}|$ and $|E_{02}|$ are taken to be the first and second atomic ionization potential, respectively. In most experiments, however, species such as neon and argon are used, for which the outer-shell electrons are in $2p$ and $3p$ states, respectively. For this reason, such states should provide a more realistic modeling of laser-induced nonsequential double ionization. For symmetry reasons, only the states with magnetic quantum number $m = 0$ will contribute to the yield.

In this case, the bound-state wave functions of both electrons will be given by

$$\psi_{210}^{(n)}(r_n) = C_{210} r_n \exp[-\alpha r_n] \cos \theta \quad (19)$$

and

$$\psi_{310}^{(n)}(r_n) = C_{310} r_n (1 - \alpha r_n / 2) \exp[-\alpha r_n] \cos \theta, \quad (20)$$

respectively, where $\alpha = \sqrt{2|E_{0n}|}$ and C_{n10} ($n = 1, 2$) denote normalization constants. For comparison, we will also consider hydrogenic 1s wave functions, which read

$$\psi_{100}^{(n)}(r_n) = C_{100} \exp[-\alpha r_n]. \quad (21)$$

In Eqs. (19)-(21), the binding energies of the first and the second electron were chosen as the first and the second ionization potentials, respectively.

A. Contact-type interaction

As a first step, we will assume that the second electron is released by a contact-type interaction

$$V_{12} = \delta(\mathbf{r}_1 - \mathbf{r}_2). \quad (22)$$

In this case, the form factors $V_{\mathbf{p}_n, \mathbf{k}}$, for $2p$ and $3p$ initial states, read

$$V_{\mathbf{p}_n, \mathbf{k}} \sim \frac{\tilde{p}}{[2|E_{02}| + \tilde{\mathbf{p}}^2]^3} \quad (23)$$

and

$$V_{\mathbf{p}_n, \mathbf{k}} \sim \frac{\tilde{p}(\tilde{\mathbf{p}}^2 - 2|E_{02}|)}{[2|E_{02}| + \tilde{\mathbf{p}}^2]^4}, \quad (24)$$

respectively, with $\tilde{\mathbf{p}} = \mathbf{p}_1 + \mathbf{p}_2 - \mathbf{k} + \mathbf{A}(t)$. The corresponding form factor obtained for an initial state (21) is given by

$$V_{\mathbf{p}_n, \mathbf{k}} \sim \frac{1}{[2|E_{02}| + \tilde{\mathbf{p}}^2]^2}. \quad (25)$$

The differential electron momentum distributions computed with such form factors are depicted in Figs. 1(a)-1(c), as contour plots in the $(p_{1||}, p_{2||})$ plane. In such computations, only the pair of orbits for which the electron excursion times $\tau = t - t'$ in the continuum are shortest have been employed. As an overall feature, the distributions are peaked near $p_{1||} = p_{2||} = \pm\sqrt{U_p}$ and spread in the direction perpendicular to the diagonal $p_{1||} = p_{2||}$.

An inspection of the form factors (23)-(25) explains this behavior. Indeed, such form factors are large if $\tilde{\mathbf{p}} = \mathbf{p}_1 + \mathbf{p}_2 - \mathbf{k} + \mathbf{A}(t)$ is small. To first approximation, since the first electron returns at times t close to the minimum of the electric field, one may assume that the vector potential at this time and the intermediate electron momentum are approximately constant. Furthermore, in the model, the field is approximated by a monochromatic wave and \mathbf{k} is given by Eq. (10). Hence, a rough estimate of these quantities at the return times yields $A(t) \simeq 2\sqrt{U_p}$ and $k \simeq 0$, respectively. Thus, $\tilde{\mathbf{p}}$ will be small mainly if $\mathbf{p}_1 = -\mathbf{p}_2$, so that contributions along the anti-diagonal $p_{1||} = -p_{2||}$ will be enhanced.

Such contributions get more localized near the maxima for highly excited initial states due to the increase in the exponent of the denominator. A direct look at the above-stated form factors confirms this interpretation, yielding maxima along the anti-diagonal and near $\pm\sqrt{U_p}$.

Interestingly, the distributions obtained for the contact interaction are quite different from the circular distributions peaked around $p_{1||} = p_{2||} = \pm 2\sqrt{U_p}$ observed experimentally. Indeed, in order to obtain such distributions, it is necessary to assume that the initial wave function of the second electron is localized at $r_2 = 0$. This is formally equivalent to taking

$$V_{12}(\mathbf{r}_1 - \mathbf{r}_2)\psi_0^{(2)}(\mathbf{r}_2) \sim \delta(\mathbf{r}_1 - \mathbf{r}_2)\delta(\mathbf{r}_2). \quad (26)$$

Eq. (26) yields a constant form factor $V_{\mathbf{p}_n, \mathbf{k}}$. In Fig. 1(d), we present the distributions computed using Eq. (26), which exhibit a very good agreement with the experiments. This means that, in reality, the effective wave function of the second electron is very localized, most probably due to refocussing [22], or screening effects [28].

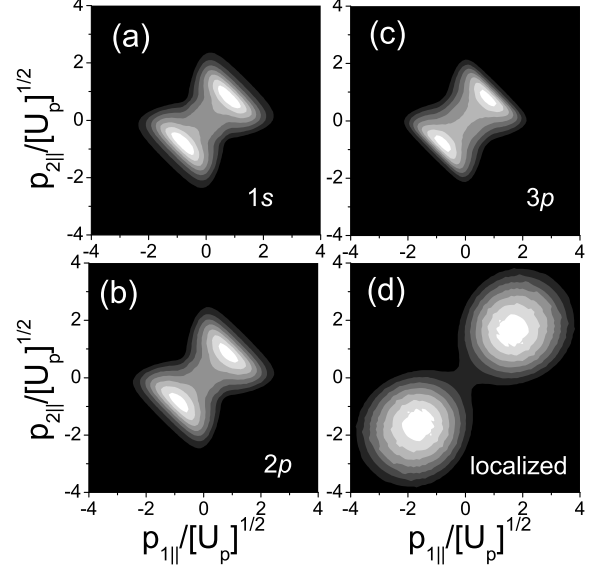


FIG. 1: Electron momentum distributions computed using a contact-type interaction, as functions of the electron momentum components parallel to the laser-field polarization. The external field was taken to be monochromatic, with frequency $\omega = 0.057$ a.u. and intensity $I = 8 \times 10^{14} \text{ W/cm}^2$. In panels (a), (b) and (c), both electrons are initially bound in a $1s$, $2p$, and $3p$ state [Eqs. (21), (19) and (20)], respectively, whereas, in part (d), the first electron is initially in a $1s$ state and the wave function of the second electron is localized at $r_2 = 0$. In all situations (even for the $3p$ -state case), the atomic species was taken to be neon ($|E_{01}| = 0.79$ a.u. and $|E_{02}| = 1.51$ a.u.), in order to facilitate a clear assessment of the effects caused by the different initial states. The transverse momenta have been integrated over.

B. Coulomb-type interaction

We will now consider that the second electron is released by a Coulomb type interaction, given by

$$V_{12} = 1/|\mathbf{r}_1 - \mathbf{r}_2|. \quad (27)$$

In this case, the form factors corresponding to initial $2p$ and $3p$ states read

$$V_{\mathbf{p}_n, \mathbf{k}} \sim \frac{1}{[\mathbf{p}_1 - \mathbf{k}]^2} \frac{\tilde{p}}{[2|E_{02}| + \tilde{\mathbf{p}}^2]^3} + \mathbf{p}_1 \leftrightarrow \mathbf{p}_2 \quad (28)$$

and

$$V_{\mathbf{p}_n, \mathbf{k}} \sim \frac{1}{[\mathbf{p}_1 - \mathbf{k}]^2} \frac{\tilde{p}(\tilde{\mathbf{p}}^2 - 2|E_{02}|)}{[2|E_{02}| + \tilde{\mathbf{p}}^2]^4} + \mathbf{p}_1 \leftrightarrow \mathbf{p}_2, \quad (29)$$

respectively, and are largest when $\tilde{\mathbf{p}}$ or $\mathbf{p}_1 - \mathbf{k}$ are small. This trend was already present in the $1s$ -state case [15, 16], for which

$$V_{\mathbf{p}_n, \mathbf{k}} \sim \frac{1}{[\mathbf{p}_1 - \mathbf{k}]^2 [2|E_{02}| + \tilde{\mathbf{p}}^2]^2} + \mathbf{p}_1 \leftrightarrow \mathbf{p}_2. \quad (30)$$

The influence of such form factors on the electron momentum distributions is shown in Fig. 2. Apart from the broadening along $p_{1||} = -p_{2||}$ caused by the spatial extent of the bound-state wave functions (c.f. Sec. III A), the distributions exhibit maxima near the axis $p_{1||} = 0$ or $p_{2||} = 0$. Such maxima are due to the factor $[\mathbf{p}_n - \mathbf{k}]^{-2}$ ($n = 1, 2$) in Eqs. (28)-(30), characteristic of the Coulomb-type interaction, which is large for $\mathbf{p}_n \simeq \mathbf{k}$. Since, to first approximation, contributions from regions of small k dominate the yield, one expects maxima in momentum regions where either \mathbf{p}_1 or \mathbf{p}_2 are small.

Furthermore, as compared to the yields obtained using a Coulomb-type interaction and $1s$ -states, there exists a small additional broadening in the distributions, with respect to the diagonal $p_{1||} = p_{2||}$, as well as an increase in the contributions from regions where such momenta are small. Such effects get more pronounced as the principal quantum number increases, as shown in Figs. 2.(b) and 2.(c). This broadening is not specific to p states, and occurs due to the fact that the initial electronic bound states extend over a larger spatial region, as the principal quantum number increases.

However, such modifications do not alter the distributions in a significant way. More extreme changes occur, for instance, if a contact-type interaction, i.e., Eq. (22), is taken into account. Still, less localized bound states for both electrons will cause a broadening in the momentum distributions. If the second-electron wave function is localized at the origin, the form factor (30) reduces to

$$V_{\mathbf{p}_n, \mathbf{k}} \sim \frac{1}{[\mathbf{p}_1 - \mathbf{k}]^2} + \mathbf{p}_1 \leftrightarrow \mathbf{p}_2. \quad (31)$$

The distributions for the latter form factor are displayed in Fig. 2.(d). In the figure, one observes a considerable reduction of the broadening along the anti-diagonal $p_{1||} = -p_{2||}$. However, the distributions still exhibit the two sets of maxima near the axis $p_{1||} = 0$ or $p_{2||} = 0$. This is expected, since such maxima are a fingerprint of the Coulomb interaction.

The results in this section show that the shapes of the momentum distributions in NSDI are not only influenced by the type of interaction by which the second electron is dislodged but, additionally, depend on the spatial extension of the wave function of the state where it is initially bound. In fact, radically different shapes are observed if this wave function is either taken to be localized at $\mathbf{r}_2 = 0$ or exponentially decaying. This is true both for a contact- and a Coulomb-type interaction (c.f. Figs. 1.(d) and 2.(d)).

On the other hand, if different initial states are taken, for the same type of interaction, there are no significant changes in the shapes of the distributions as long as such states extend over a finite spatial range. This is explicitly seen by comparing yields obtained using bound states with different principal quantum numbers. This is related to the fact that the wave functions (19)-(21) were chosen such that the bound-state energy always corresponds to the second ionization potential. Hence, even if

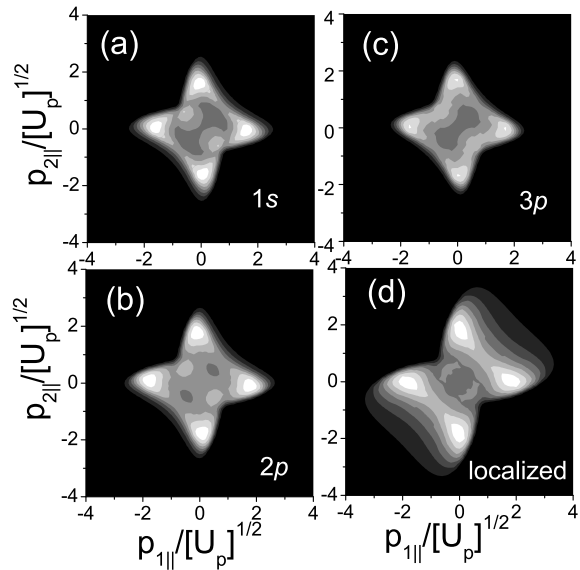


FIG. 2: Electron momentum distributions computed using a Coulomb-type interaction, as functions of the electron momentum components parallel to the laser-field polarization. The field and atomic parameters are the same as in Fig. 1. In panels (a), (b) and (c), both electrons are taken to be initially in a $1s$, $2p$, and $3p$ state, respectively, whereas in panel (d) the first electron is in a $1s$ state, while the spatial extension of the bound-state wave function has been neglected. The transverse momenta have been integrated over.

their shape changes, the spatial extension of such wave functions is roughly the same.

It is still, however, quite puzzling that the best agreement with the experimental findings occurs for the crudest approximations, both for the interaction and the initial bound-state wave function, i.e., for a contact-type interaction and a wave function localized at $\mathbf{r}_2 = 0$. Indeed, taking either a more realistic type of electron-electron interaction, spatially extended bound states, or, still, bound states which are, in principle, a more refined description of the outer-shell electrons, only worsens the agreement between experiment and theory.

If the main physical mechanism of NSDI is electron-impact ionization, there exist two main possibilities for explaining this discrepancy. Either the second electron is bound in highly localized states and collide through an effective short-range interaction, as the present results suggest, or the tunneling ionization, as well as the electron propagation in the continuum, must be improved. The first issue may be addressed by including the influence of the residual ion in the process, whereas the second issue may be dealt with in several ways. For instance, in the subsequent section, we will consider corrections of a more fundamental nature, which alter the semiclassical action and thus the orbits of the electrons.

IV. TREATMENT OF THE BOUND-STATE SINGULARITY

Up to the present section, we have implicitly assumed that the form factors $V_{\mathbf{p}_1, \mathbf{p}_2, \mathbf{k}}$ and $V_{\mathbf{k}, 0}$ are free of singularities and slowly varying in comparison to the time-dependent action. However, this is not always true. Indeed, in the saddle-point framework, the form factor $V_{\mathbf{k}, 0}$ is singular if the electron is initially in a state described by an exponentially decaying wave function, such as Eqs. (19)-(21). More specifically, in this case,

$$V_{\mathbf{k}, 0} \propto \frac{f(k + A(t'))}{([\mathbf{k} + \mathbf{A}(t')]^2 + 2|E_{01}|)^n}, \quad (32)$$

for which the denominator vanishes, according to Eq. (8). Due to this singularity, this form factor does not vary slowly with respect to the semi-classical action (3), and thus must be incorporated in the exponent. Therefore, we take the modified action

$$\tilde{S}(t, t', \mathbf{p}_n, \mathbf{k}) = S(t, t', \mathbf{p}_i, \mathbf{k}) - i \ln[V_{\mathbf{k}, 0}] \quad (33)$$

in the transition amplitude (2). This causes a change in the first and third saddle-point equations, which will depend on the initial bound state in question. In particular, we will consider that the first electron is initially in the hydrogenic states $1s$, $2p$, and $3p$. This is a legitimate assumption, since the binding potential of a neutral atom, from which the first electron tunnels out, is of long-range type. For the states $1s$, $2p$, and $3p$, $V_{\mathbf{k}, 0}$ reads

$$V_{\mathbf{k}, 0}^{(1s)} = \frac{\sqrt{2}}{\pi} \frac{(2|E_{01}|)^{5/2}}{\mathbf{v}^2 + 2|E_{01}|}, \quad (34)$$

$$V_{\mathbf{k}, 0}^{(2p)} = \frac{2\sqrt{2}i}{\pi} \frac{(\sqrt{2|E_{01}|})^{5/2}v}{(\mathbf{v}^2 + 2|E_{01}|)^2}, \quad (35)$$

and

$$V_{\mathbf{k}, 0}^{(3p)} = \frac{8i(\sqrt{2|E_{01}|})^{5/2}v(\mathbf{v}^2 - 2|E_{01}|)}{\sqrt{3}\pi(\mathbf{v}^2 + 2|E_{01}|)^3}, \quad (36)$$

respectively, where $\mathbf{v} = [\mathbf{k} + \mathbf{A}(t')]$ denotes the initial electron drift velocity. The explicit expressions for the saddle point equations then become

$$[\mathbf{k} + \mathbf{A}(t')]^2 = -2|E_{01}| + \zeta(k, t') \cdot \mathbf{E}(t') \quad (37)$$

and

$$\int_{t'}^t d\tau [\mathbf{k} + \mathbf{A}(\tau)] + \zeta(k, t') = 0, \quad (38)$$

respectively, where $\zeta(k, t') = -i\partial_{\mathbf{k}} \ln[V_{\mathbf{k}, 0}]$ is a correction which depends on the initial bound state. Thus, there is an effective shift in the ionization potential at the tunneling times, and a modification in the return condition.

Consequently, there is change in the orbits. Apart from that, from the technical point of view, the transition amplitude is no longer reducible to a two-dimensional integral, so that the problem is far more cumbersome.

The modifications in the equation describing tunneling ionization allow the existence of solutions for which $\text{Re}[v] \neq 0$. This did not occur in Eq. (8), for which this quantity was purely imaginary, and, physically, means that there are in principle changes, maybe even enhancements, in the probability that the first electron tunnels out at t' .

Furthermore, Eq. (38), if written in terms of the components of the intermediate momentum \mathbf{k} parallel and perpendicular to the laser field polarization, has, apart from the trivial solution $\mathbf{k}_{\perp} = 0$, additional solutions for which $\mathbf{k}_{\perp} \neq 0$. Thus, in principle, the first electron may have a non-vanishing drift velocity component transverse to the laser-field polarization. We regard this possibility, however, as non-physical, and therefore will mainly concentrate on the case of vanishing \mathbf{k}_{\perp} . Despite of that, the results obtained for nonvanishing \mathbf{k}_{\perp} will be briefly discussed in Sec. IV B. For the return condition (9) this is not possible and \mathbf{k}_{\perp} is always vanishing. In the following, we will investigate how the corrections in the action affect the momentum distributions.

A. Vanishing \mathbf{k}_{\perp}

In this section, we will consider that the first electron has vanishing intermediate momentum components \mathbf{k}_{\perp} . Physically, this means that the dynamics of NSDI is mainly taking place along the laser field polarization, which is the intuitively expected situation. In Fig. 3, we present the electron momentum distributions computed employing the modified saddle-point equations and the action (33), for the same initial states and types of as in Figs. 1 and a contact-type interaction. In general, the distributions in Fig. 3 are very similar to the former ones, with, however, a suppression in the region of small parallel momenta. This is true even if different corrections are taken into account, as it is the case if the first electron is initially in a $1s$, $2p$ and $3p$ state (Figs. 3.(a), 3.(b) and 3.(c), respectively). In the specific case of a localized bound-state wave function for the second electron, there is also a minor displacement of the maxima towards smaller parallel momenta(c.f. Fig. 3(d)).

The suppression persists if the second electron is released by a Coulomb-type interaction, as shown in Fig. 4. Specifically for this interaction, the corrections lead to a suppression of the secondary maxima in the small-momentum region, which were present in Fig. 2.

In the following, we will analyze these differences in terms of the so-called quantum orbits, obtained by solving the saddle point equations. We will consider both the saddle-point equations in the presence and absence of corrections to the bound-state singularity, i.e., Eqs. (37), (9) and (38), and (8)-(10), respectively. We re-

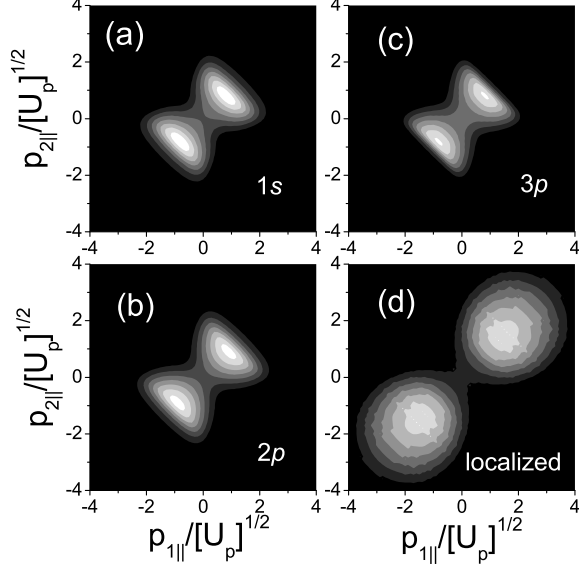


FIG. 3: Electron momentum distributions computed with using contact-type interaction, as functions of the electron momentum components parallel to the laser-field polarization, for the same field and atomic parameters as in the previous figures. We introduce corrections to the bound-state singularity by employing the modified action (33) and saddle-point equations, taking the solutions displayed in Figs. 6.(a) and 6.(c). In panels (a), (b) and (c), both electrons are taken to be initially in a $1s$, in a $2p$, and in a $3p$ state, respectively, whereas in panel (d) the first electron is initially in a $1s$ state, while the spatial extension of the bound-state wave function of the second electron has been neglected. The transverse momenta have been integrated over.

strict ourselves to vanishing final transverse momenta and longitudinal momentum components along the diagonal $p_{||} = p_{1||} = p_{2||}$. For this particular case, the energy region for which electron-impact ionization is classically allowed is most extense.

In Fig. 5, we display the solutions of the saddle-point equations for the rescattering times t and the intermediate momentum \mathbf{k} . The upper and lower panels in the figure give the real and imaginary parts of such variables, respectively. The real parts of t and \mathbf{k} correspond to the solutions of the equations of motion of a classical electron in an external laser field, and almost merge at two distinct parallel momenta. These momenta are related to the maximal and minimal energy for which the second electron is able to overcome $|E_{02}|$. Beyond such momenta, there are cutoffs in the distributions, and the yield decays exponentially. The imaginary parts of such variables are in a sense a measure of a particular physical process being classically allowed and forbidden. Indeed, the fact that $|\text{Im}[t]|$ and $|\text{Im}[k]|$ are vanishingly small between the minimal and maximal allowed momenta are a consequence of both electron-impact ionization and the return

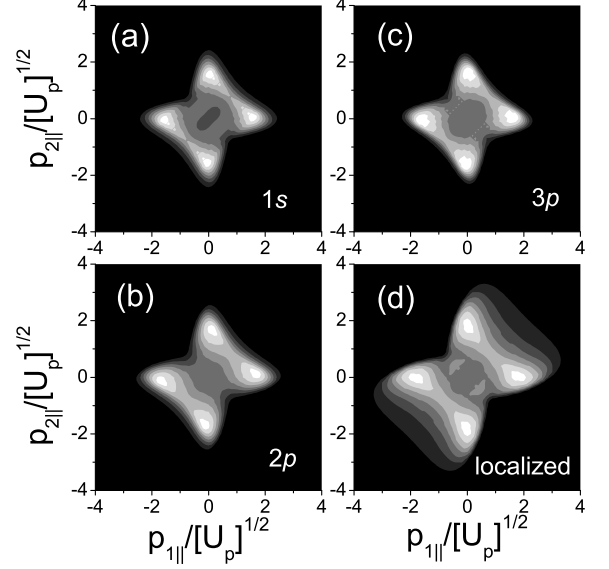


FIG. 4: Electron momentum distributions computed using the Coulomb-type interaction, as functions of the electron momentum components parallel to the laser-field polarization, for same field and atomic parameters as in the previous figure. We introduce corrections to the bound-state singularity by employing the modified action (33) and saddle-point equations, and the solutions in Figs. 6.(a) and 6.(c). In panels (a), (b) and (c), both electrons are taken to be initially in a $1s$, in a $2p$, and in a $3p$ state, respectively, whereas in panel (d) the first electron is initially in a $1s$ state, while the spatial extension of the bound-state wave function of the second electron has been neglected. The transverse momenta have been integrated over.

condition being classically allowed in this region. As the boundaries of this region are reached, $|\text{Im}[t]|$ and $|\text{Im}[k]|$ increase exponentially. Interestingly, both the real and imaginary parts of such variables, as well as the cutoff momenta, remain practically inalterd upon the changes introduced in this section. This is not obvious, since the bound-state corrections in question alter the return condition [c.f. Eq.(38)].

There exist, however, modifications in the tunneling times t' , which are explicitly shown in Fig. 6. Specifically, the corrections in the tunneling condition, which leads to Eq. (37), cause a splitting in the solutions of Eq. (8). This follows from the fact that small variations in the stationary-action trajectories contributes quadratically to $S(t, t', \mathbf{p}_n, \mathbf{k})$ and $V_{\mathbf{k},0}$, so that $\tilde{S}(t, t', \mathbf{p}_n, \mathbf{k})$ attains two stationary trajectories for each of the former ones. Strictly speaking, a similar splitting also occurs for \mathbf{k} and t . In practice, however, the difference between the two different sets of solutions is vanishingly small, and thus not noticeable in Fig. 5. The different sets of solutions are depicted in Figs. 6.(a) and 6.(c), and 6.(b) and 6.(d), respectively. The real parts $\text{Re}[t']$ ex-

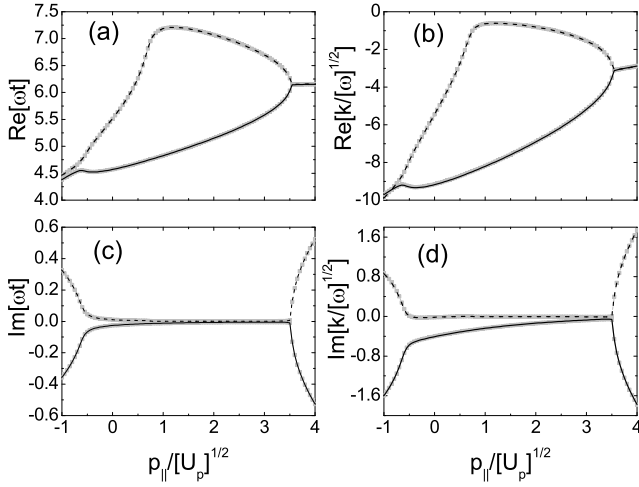


FIG. 5: Rescattering times, together with the intermediate momentum $k_{||}$, as functions of the parallel momentum $p_{||}$ along the diagonal $p_{1||} = p_{2||}$. The final transverse momenta $\mathbf{p}_{n\perp}$ ($n = 1, 2$) and the intermediate transverse momentum \mathbf{k}_{\perp} are taken to be vanishing. The real and imaginary parts of such quantities are displayed in the upper [(a), (b) and (c)] and lower [(d), (e) and (f)] panels, respectively. The field and atomic parameters are the same as in the previous figure. The uncorrected variables are given by the thick light gray curves in the figure, while the variables with corrections corresponding to initial $1s$, $2p$ and $3p$ states are given by the gray, dark gray and black curves, respectively. The longer and the shorter orbit are indicated by dashed and solid lines, respectively.

hibit only minor differences, which occur for the shorter orbits and small momenta and eventually disappear as the upper cutoff is approached. Depending on the type of correction, such times either distance themselves from, or become slightly closer to the peak-field times (Figs. 6.(a) and 6.(b), respectively). Thus, one could expect an enhancement in the contributions from the shorter orbits near the origin of the $(p_{1||}, p_{2||})$ plane, in the former case, and a suppression in the latter case. However, we have used the solutions in Fig. 6.(b) and (d) for computing the contour plots in Figs. 3 and 4, and obtained a suppression in the yield. This is a clear indication that the changes in $\text{Im}[t']$ and in the time-dependent action play a more important role than those in $\text{Re}[t']$.

In Figs. 6.(c) and 6.(d), we present the imaginary parts of t' , which clearly shift towards smaller, and larger values, respectively, when the corrections $\varsigma(k, t')$ are taken into account. The higher the initial state lies, the larger such shifts are. Physically, there exists a correspondence between such imaginary parts and the probability that the first electron tunnels out and reaches the continuum. This means that, by using a slightly modified action in order to overcome the Coulomb singularity, one is changing the effective potential barrier at t' for the first electron. In general, such a barrier has a significant influence on the distributions. Indeed, recently, we have shown, within the context of nonsequential double ion-

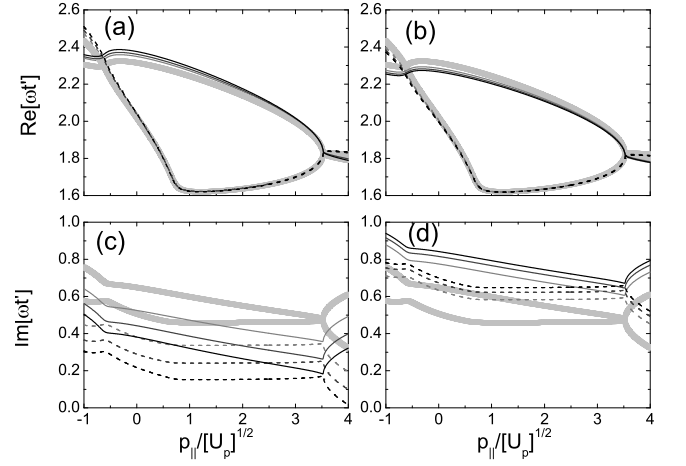


FIG. 6: Tunneling times as functions of the parallel momentum $p_{||}$ along the diagonal $p_{1||} = p_{2||}$. The final transverse momenta $\mathbf{p}_{n\perp}$ ($n = 1, 2$) and the intermediate transverse momentum \mathbf{k}_{\perp} are taken to be vanishing. The real and imaginary parts of such quantities are displayed in the upper [(a) and (b)] and lower [(c) and (d)] panels, and the same pairs of orbits are depicted in the left [(a) and (c)] and right [(b) and (d)] panels, respectively. The field and atomic parameters are the same as in the previous figure. The uncorrected variables are given by the thick light gray curves in the figure, while the variables with corrections corresponding to initial $1s$, $2p$ and $3p$ states are given by the gray, dark gray and black curves, respectively. The longer and the shorter orbit are indicated by dashed and solid lines, respectively.

ization with few-cycle laser pulses, that the importance of the contributions of a particular orbit or set of orbits to the yield is highly dependent on $|\text{Im}[t']|$. The smaller this quantity is, the larger is the tunneling probability for the first electron [17]. As a direct consequence, contributions from orbits with small $|\text{Im}[t']|$, i.e., with a large tunneling probability, dominate the yield. In the present case, however, since both orbits are being equally shifted, this should not influence the distributions qualitatively. One should note that, even in the momentum region for which electron-impact ionization is allowed, $|\text{Im}[t']|$ is always nonvanishing. This is a direct consequence of the fact that tunneling ionization is a classically forbidden process.

Subsequently, we compute the counterparts of Fig. 3 and 4 (Figs. 7 and 8) using the solutions displayed in Fig. 6.(b) and 6.(d). Also in this case, in general, there is a suppression in the yield in the region of small parallel momenta, with, however, a slightly different substructure in the Coulomb-interaction case.

B. Nonvanishing \mathbf{k}_{\perp}

The modifications introduced in the return condition for the first electron [Eq. (38)] allow the intermediate momentum \mathbf{k} to have a nonvanishing component per-

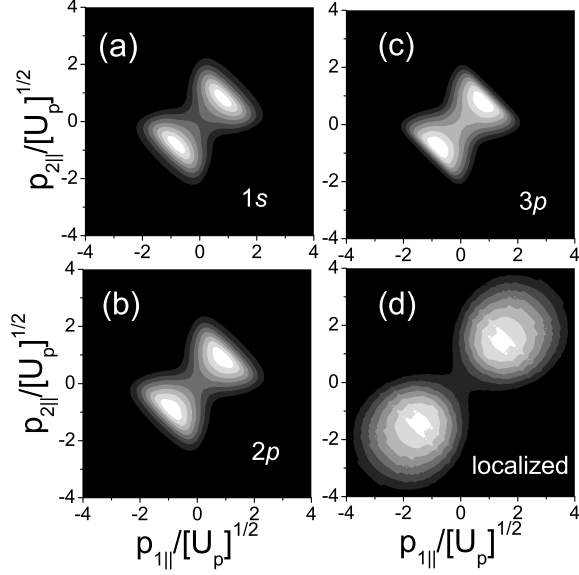


FIG. 7: Electron momentum distributions computed with using contact-type interaction, as functions of the electron momentum components parallel to the laser-field polarization, for the same field and atomic parameters as in the previous figure. We introduce corrections to the bound-state singularity by employing the modified action (33) and saddle-point equations, taking the solutions in Figs. 6.(b) and 6.(d). In panels (a), (b) and (c), both electrons are taken to be initially in a $1s$, in a $2p$, and in a $3p$ state, respectively, whereas in panel (d) the first electron is in a $1s$ state, and spatial extension of the bound-state wave function of the second electron has been neglected. The transverse momenta have been integrated over.

pendicular to the laser-field polarization. This implies that the first electron, during tunneling ionization and when it returns, is being deviated from its original direction. Although such an effect is unphysical, we will briefly discuss its consequences. For that purpose, we will consider the simplest corrections to the bound-state singularity discussed in this paper, namely those for $1s$ initial states. If Eq. (38) is written in terms of the intermediate-momentum components \mathbf{k}_\perp and k_\parallel perpendicular and parallel to the laser-field polarization, this equation reads

$$k_\parallel(t-t') - \int_{t'}^t A(s)ds + \frac{2i[k_\parallel + A(t')]}{[2|E_{01}| + \mathbf{k}_\perp^2 + [k_\parallel + A(t')]^2]} = 0 \quad (39)$$

and

$$\mathbf{k}_\perp^2 \left(t - t' + \frac{2i}{[2|E_{01}| + \mathbf{k}_\perp^2 + [k_\parallel + A(t')]^2]} \right) = 0, \quad (40)$$

respectively. Apart from the trivial solution $\mathbf{k}_\perp = 0$, the condition (40) can be satisfied by nonvanishing values of

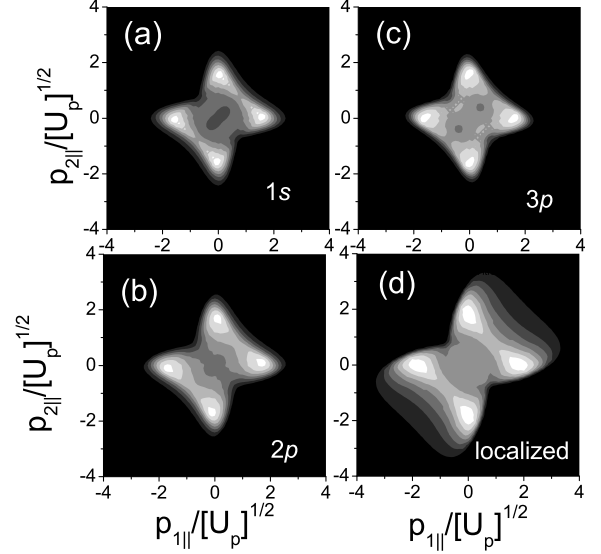


FIG. 8: Electron momentum distributions computed using the Coulomb-type interaction, as functions of the electron momentum components parallel to the laser-field polarization, for same field and atomic parameters as in the previous figure. We introduce corrections to the bound-state singularity by employing the modified action (33) and saddle-point equations, and the solutions in Figs. 6.(b) and 6.(d). In panels (a), (b) and (c), both electrons are taken to be initially in a $1s$, in a $2p$, and in a $3p$ state, respectively, whereas in panel (d) the first electron is initially in a $1s$ state, while the spatial extension of the bound-state wave function of the second electron has been neglected. The transverse momenta have been integrated over.

this variable. One should note that, in the case without corrections, this does not hold and only the trivial solution exists.

Fig. 8 depicts the tunneling and rescattering times for this case, together with the perpendicular and parallel components of \mathbf{k} . The real parts of such variables correspond, as in the previous cases, to a longer and a shorter orbit. The momenta, however, for which such orbits nearly coalesce, are radically different from those in the previous cases discussed in this paper. This is due to the fact that a nonvanishing \mathbf{k}_\perp also affects the rescattering condition (9), which now reads

$$\sum_{n=1}^2 [p_{n\parallel} + A(t)]^2 = [k_\parallel + A(t)]^2 + \mathbf{k}_\perp^2 - 2|E_{02}| - \sum_{j=1}^2 \mathbf{p}_{n\perp}^2$$

For constant final transverse momenta $\mathbf{p}_{n\perp}$ ($n = 1, 2$), this equation describes a circle centered at $-A(t)$ whose radius has been altered in \mathbf{k}_\perp^2 . Since, as shown in Figs 8(a)-8(d), this radius decreased, \mathbf{k}_\perp is expected to be almost purely imaginary. This is indeed the case, as can be seen comparing panels (d) and (h) in the figure. The imaginary parts of such variables also behave follow-

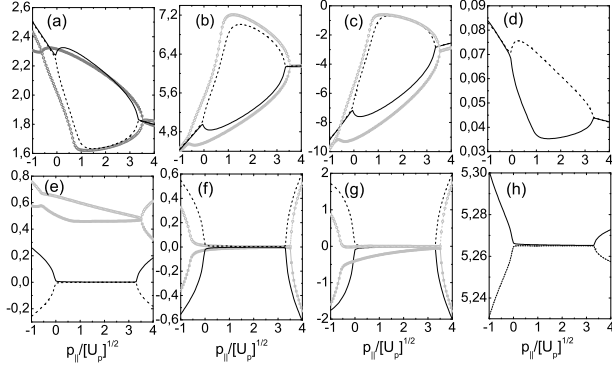


FIG. 9: Tunneling [Panels (a) and (e)] and rescattering times [Panels (b) and (f)], together with the parallel [Panels (c) and (g)] and perpendicular components of the intermediate momentum \mathbf{k} [Panels (d) and (h)], as functions of the parallel momentum $p_{||}$ along the diagonal $p_{1||} = p_{2||}$. The final transverse momenta $\mathbf{p}_{n\perp}$ ($n = 1, 2$) are taken to be vanishing. The real and imaginary parts of such quantities are displayed in the upper [(a), (b), (c) and (d)] and lower [(e), (f), (g) and (h)] panels, respectively. The field and atomic parameters are the same as in the previous figure. The corrected and uncorrected yields are given by the black and gray curves in the figure, respectively. The tunneling and rescattering times are multiplied by ω and the intermediate momenta divided by $\sqrt{\omega}$, respectively, so that a direct comparison with Figs. 5 and 6 can be performed.

ing the same pattern as previously, growing vary rapidly at the momenta for which the real parts approach each other, and remaining nearly constant inbetween. Interestingly, $\text{Im}[t']$ is vanishing in this region. This feature is in clear contradiction with the fact that tunneling is a process which is always forbidden, and therefore requires a nonvanishing $\text{Im}[t']$ (c.f. Fig. 5.(d)). For this reason, we will not use solutions with nonvanishing \mathbf{k}_{\perp} for computing electron momentum distributions.

V. CONCLUSIONS

In this paper, we investigate the influence of the initial bound-state wave functions for the first and second bound electrons, on the differential electron momentum distributions for laser-induced nonsequential ionization. We employ a quantum-mechanical S-Matrix model within the Strong-Field Approximation, in which this phenomenon is described as the inelastic collision of the first electron with its parent ion. The second electron is then freed by electron-impact ionization. In particular, we compute the NSDI transition amplitudes using a uniform approximation, which is closely related to path-integral methods, and interpret the results in terms of the so-called "quantum orbits". Such orbits are closely related to the orbits of classical electrons recolliding with

their parent ion. We consider that the second electron is dislodged by a contact- and Coulomb-type interaction, and assume that both electron are initially in a $1s$, $2p$ or $3p$ hydrogenic state. As an additional case, we consider that the first electron is initially bound in a $1s$ state, and that the initial wave function of the second electron is localized at $\mathbf{r}_2 = 0$.

Concerning the initial bound-state wave function of the second electron, our results show that the NSDI momentum distributions are very sensitive to its spatial extension, but not to its shape. Indeed, a spatially extended wave function causes a broadening in the electron momentum distributions along the anti-diagonal $p_{1||} = -p_{2||}$, even if the second electron is dislodged by a contact-type interaction. Circular-shaped distributions, as reported in [15, 16] and observed in experiments [1, 3] are only obtained for a contact-type interaction under the additional condition that the bound-state wave function is localized at the origin of the coordinate system, i.e., at $\mathbf{r}_2 = 0$. In addition to this broadening, if the second electron is released by a Coulomb-type interaction, there is an enhancement in the contributions near the axis $p_{1||} = 0$ or $p_{2||} = 0$.

All the distributions investigated in this article, however, change in a less radical fashion if the second electron is taken to be in a $1s$, $2p$ or $3p$ hydrogenic state, as long as they exhibit a spatial extension. In fact, although specific changes are observed, such as an additional substructure for a Coulomb-type interaction, or more localized distributions for a contact-type interaction, the overall shapes of such distributions remains similar.

Furthermore, if the form factor $V_{\mathbf{k},0}$, which, within our model, contains all the influence of the initial state of the first electron, is incorporated in the time-dependent action, the only noticeable effect is a suppression in the yield, for regions of small parallel momenta. Indeed, the distributions retain their shapes even if the saddle-point equations are modified in this way. Such changes have been introduced in order to correct a singularity which exists for such the prefactor $V_{\mathbf{k},0}$, within the saddle-point framework, if the initial bound state is exponentially decaying.

Finally, it is very intriguing that the most simplified model, i.e., a contact-type interaction localized at the origin of the coordinate system, yields the best agreements with the experimental findings. Indeed, all the technical modifications considered in this paper, which aimed at making the model more realistic, either worsened this agreement, or had almost no influence on the momentum distributions. Similar conclusions have also been obtained in previous studies, in which final-state electron-electron repulsion has been incorporated [15, 16]. In [15, 16], we raised the hypotheses that the residual ion might be screening both the long-range of the Coulomb interaction, or the final-state Coulomb repulsion. According to the results of this paper, it appears that effects such as Coulomb focusing, which, again, owes its existence to the presence of the ion, may be compensat-

ing the broadening caused by initial spatially extended wave functions. Such a broadening occurs in the direction of the anti-diagonal $p_{1||} = -p_{2||}$, and is present even if a contact-type interaction releases the second electron. Definite statements on this issue, however, require either incorporating such an ion in our model or a theoretical approach beyond the Strong-Field Approximation.

Acknowledgments

This work was financed in part by the Deutsche Forschungsgemeinschaft (SFB 407 and European Grad-

uate College “Interference and Quantum Applications”). C.F.M.F. would like to thank the Optics Section at the Imperial College and City University for their kind hospitality.

-
- [1] See, e.g., R. Dörner, T. Weber, W. Weckenbrock, A. Staudte, M. Hattass, H. Schmidt-Böcking, R. Moshhammer, and J. Ullrich, *Adv. At. Mol. Opt. Phys.* **48**, 1 (2002); J. Ullrich, R. Moshhammer, A. Dorn, R. Dörner, L. Ph. H. Schmidt, H. Schmidt-Böcking, *Rep. Prog. Phys.* **66**, 1463 (2003) for reviews on the subject.
 - [2] R. Moshhammer, B. Feuerstein, W. Schmitt, A. Dorn, C.D. Schröter, J. Ullrich, H. Rottke, C. Trump, M. Wittman, G. Korn, K. Hoffmann, and W. Sandner, *Phys. Rev. Lett.* **84**, 447 (2000); Th. Weber, M. Weckenbrock, A. Staudte, L. Spielberger, O. Jagutzki, V. Mergel, F. Afaneh, G. Urbasch, M. Vollmer, H. Giessen, and R. Dörner, *ibid.* **84**, 443 (2000).
 - [3] B. Feuerstein, R. Moshhammer, D. Fischer, A. Dorn, C.D. Schröter, J. Deipenwisch, J.R. Crespo Lopez-Urrutia, C. Höhr, P. Neumayer, J. Ullrich, H. Rottke, C. Trump, M. Wittmann, G. Korn and W. Sandner, *Phys. Rev. Lett.* **87**, 043003 (2001); Th. Weber, H. Giessen, M. Weckenbrock, G. Urbasch, A. Staudte, L. Spielberger, O. Jagutzki, V. Mergel, M. Vollmer, R. Dörner, *Nature* **405**, 658 (2000).
 - [4] M. Yu. Kuchiev, *Pis'ma Zh. Eksp. Teor. Fiz.* **45**, 319(1987)(JETP Lett 45 (7), 404 (1987)); P. B. Corkum, *Phys. Rev. Lett.* **71**, 1994 (1993); K. C. Kulander, K. J. Schafer, and J. L. Krause in: B. Piraux et al. eds., *Proceedings of the SILAP conference*, (Plenum, New York, 1993).
 - [5] M. Lewenstein, Ph. Balcou, M. Yu. Ivanov, A. L'Huillier and P. B. Corkum, *Phys. Rev. A* **49**, 2117 (1994); W. Becker, S. Long, and J. K. McIver, *Phys. Rev. A* **41**, 4112 (1990); *ibid.* **50**, 1540 (1994).
 - [6] G. G. Paulus, W. Becker, W. Nicklich and H. Walther, *J. Phys. B* **27**, L703 (1994).
 - [7] W. Becker, A. Lohr and M. Kleber, *J. Phys. B* **27**, L325 (1994); M. Lewenstein, K. C. Kulander, K.J. Schafer and Ph. Bucksbaum, *Phys. Rev. A* **51**, 1495 (1995).
 - [8] B. Feuerstein, R. Moshhammer and J. Ullrich, *J. Phys. B* **33**, L823 (2000); J. Chen, J. Liu, L.-B. Fu, and W. M. Zheng, *Phys. Rev. A* **63**, 011404 (R)(2000); L.-B. Fu, J. Liu, J. Chen, and S.-G. Chen, *ibid.*, 043416 (2001); J. Chen, J. Liu, and S.-G. Chen, *Phys. Rev. A* **65**, 021406 (R)(2002); J. Chen, J. Liu, and W. M. Zheng, *ibid.* **66**, 043410 (2002).
 - [9] S. L. Haan, P. S. Wheeler, R. Panfili, and J. H. Eberly, *Phys. Rev. A* **66**, 061402(R) (2002); R. Panfili, S. L. Haan and J. H. Eberly, *Phys. Rev. Lett.* **89**, 113001 (2002).
 - [10] X. Liu and C. Figueira de Morisson Faria, *Phys. Rev. Lett.* **92**, 133006 (2004).
 - [11] A. Becker and F.H.M. Faisal, *Phys. Rev. A* **50**, 3256 (1994)
 - [12] A. Becker and F.H.M. Faisal, *Phys. Rev. Lett.* **89**, 193003 (2002); A. Jaron and A. Becker, *Phys. Rev. A* **67**, 035401 (2003).
 - [13] R. Kopold, W. Becker, H. Rottke and W. Sandner, *Phys. Rev. Lett.* **85**, 3781 (2000); S. P. Goreslavskii, S. V. Popruzhenko, R. Kopold and W. Becker, *Phys. Rev. A* **64**, 053402 (2002); S. V. Popruzhenko, Ph. A. Korneev, S. P. Goreslavskii, and W. Becker, *Phys. Rev. Lett.* **89**, 023001 (2002); A. Heinrich, M. Lewenstein and A. Sanpera, *J. Phys. B* **37**, 2087 (2004).
 - [14] C. Figueira de Morisson Faria and W. Becker, *Laser Phys.* **13**, 1196 (2003).
 - [15] C. Figueira de Morisson Faria, X. Liu, W. Becker and H. Schomerus, *Phys. Rev. A* **69**, 021402(R) (2004).
 - [16] C. Figueira de Morisson Faria, H. Schomerus, X. Liu, and W. Becker, *Phys. Rev. A* **69**, 043405 (2004).
 - [17] C. Figueira de Morisson Faria, X. Liu, A. Sanpera and M. Lewenstein, *Phys. Rev. A* **70**, 043406 (2004).
 - [18] L.V. Keldysh, *Zh. Éksp. Teor. Fiz.* **47**, 1945 (1964)[*Sov. Phys. JETP* **20**, 1307 (1965)]; F. H. M. Faisal, *J. Phys. B* **6**, L312 (1973); H. R. Reiss, *Phys. Rev. A* **22**, 1786 (1980).
 - [19] M. Weckenbrock, M. Hattass, A. Czasch, O. Jagutzki, L. Schmidt, T. Weber, H. Roskos, T. Löffler, M. Thomson and R. Dörner, *J. Phys. B* **34**, L449 (2001); R. Moshhammer, B. Feuerstein, J. Crespo López-Urrutia, J. Deipenisch, A. Dorn, D. Fischer, C. Höhr, P. Neumayer, C.D. Schröter, J. Ullrich, H. Rottke, C. Trump, M. Wittmann, G. Korn, and W. Sandner, *Phys. Rev. A* **65**, 035401 (2002).
 - [20] J.B. Watson, A. Sanpera, D. G. Lappas, P. L. Knight and K. Burnett, *Phys. Rev. Lett.* **78**, 1884 (1997); D. Dundas, K. T. Taylor, J. S. Parker, and E. S. Smyth, *J. Phys. B* **32**, L231 (1999); W. C. Liu, J. H. Eberly, S. L. Haan, R. Grobe, *Phys. Rev. Lett.* **83**, 520 (1999); C. Szymanowski, R. Panfili, W. C. Liu, S. L. Haan, and J. H. Eberly, *Phys. Rev. A* **61**, 055401 (2000); M. Lein, E. K. U. Gross, and V. Engel, *Phys. Rev. Lett.* **85**, 4707 (2000).
 - [21] See, e.g., P. Salières, B. Carré, L. Le Deroff, F. Grasbon,

- G. G. Paulus, H. Walther, R. Kopold, W. Becker, D. B. Milošević, A. Sanpera and M. Lewenstein, *Science* **292**, 902 (2001); W. Becker, F. Grasbon, R. Kopold, D.B. Milošević, G.G. Paulus, and H. Walther, *Adv. At. Mol. Opt. Phys.***48**, 35 (2002) and references therein.
- [22] G. L. Yudin, and M. Yu. Ivanov, *Phys. Rev. A* **63**, 033404 (2001).
- [23] M. V. Berry, *Proc. R. Soc. Lond. A* **422**, 7 (1989)
- [24] C. Figueira de Morisson Faria, H. Schomerus and W. Becker, *Phys. Rev. A* **66**, 043413 (2002).
- [25] D. B. Milošević, and W. Becker, *Phys. Rev. A* **66**, 063417 (2004); G. Sansone, C. Vozzi, S. Stagira and M. Nisoli, *Phys. rev. A* **70**, 013411 (2004); L.E. Chipperfield, L.N. Gaier, P.L. Knight, J. P. Marangos, and J.W.G. Tisch, submitted to *J. Mod. Opt.*
- [26] N. Bleistein and R. A. Handelsman, *Asymptotic Expansions of Integrals* (Dover, New York, 1986).
- [27] H. Schomerus and M. Sieber, *J. Phys. A* **30**, 4537(1997)
- [28] This effect can be described employing the Hartree-Fock approximation to compute bound states of neon, or argon. For a discussion of this method, see, e.g., H. Bethe and E.E. Salpeter, *Quantum Mechanics of One and Two electron Atoms*, (Plenum, New York, 1997); for applications of HF potentials for time dependent problems see K.C. Kulander, *Phys. Rev. A* **36**, 2726 (1987); *ibid.* **38**, 777 (1988); M.S. Pindzola, D.C. Griffin, and C. Bottcher, *Phys. Rev. Lett.* **66**, 2305 (1991).